Temp Title: Diffractive dissociation in a minijet model

M. Broilo,* V. P. Gonçalves,† and P. V. R. G. Silva‡
High and Medium Energy Group,
Instituto de Física e Matemática,
Universidade Federal de Pelotas
Caixa Postal 354, CEP 96010-900, Pelotas, RS, Brazil
(Dated: July 7, 2020)

We explore an update of the Lipari-Lusignoli model for multiple parton interaction in proton-pronton (pp) and antiproton-proton ($\bar{p}p$) collisions considering the recently released LHC precise measurements at $\sqrt{s} = 13$ TeV. By means of a multi-channel eikonal model where diffractive dissociation is obtained using the Good-Walker approach, we give predictions to the total as well as elastic and diffractive cross sections where the soft sector is written based on Regge-Gribov phenomenology and the hard sector is given by the usual perturbative QCD cross-section with updated sets of parton distribuition functions.
Conferir quais outros PACs devem ser adicionados

PACS numbers: 13.85.Dz, 13.85.Lg

I. INTRODUCTION

The field of research on Hadron Physics is one of the most interesting and challenging in this precision High-Energy LHC-Era that we are presently living in. Very recently the TOTEM experiment at the LHC has released precise measurements of proton-proton elastic, inelastic and total cross sections as well as measurements of the ratio of the real-to-imaginary part of the forward elastic scattering amplitude, *a.k.a.* ρ-parameter [1–4]. Up so forth these measurements represent the highest center-of-mass (CM) energy ever achieved in a collider. Over the last few years an intense debate has enhanced the interest in the subject and become a key source of information for selecting phenomenological models and theoretical approaches to understand, in a deeper level, the theory of strong interactions. Presently, it is widely known that total, elastic and inelastic cross sections rise with increasing energy [5, 6] and also that most of the contribution comes from processes with low transferred momenta. Moreover, diffractive reactions can not be treated perturbatively and calculated in a reliable way within Quantum Chromodynamics (QCD). This constitutes the *kernel* of one of the more basic and still open problems in strong interaction: the description of hadronic cross sections.

A wide variaty of models in high-energy particle scattering belong to the so-called class of minijet models or also named QCD-inspired models. These type of models represent an attempt to create a solid background towards a future description fully based on QCD. Moreover, they aim to describe some hadronic procceses linked to the transition region between the perturbative and nonperturbative domains by means of the QCD parton model [7]. Nonetheless, in the theoretical QCD concept, the deep infrared region, *i.e.* for asymptotically $t \to 0$, one does not expect to be accessed by perturbative techniques only, and to be able to predict the hadronic cross sections energy-dependence without model assumptions. In this way Regge-Gribov phenomenology represents a whole class of s-channel models which are used to investigate the asymptotic behavior of the forward and nonforward elastic scattering amplitudes. Over the last decades, many methods were propose based on Regge-Gribov theory or inspired on QCD, *cf.* [8–35], which were able, in most cases, to give a fine description of the pre [36] and post-LHC [1–4, 37–42] bulk of experimental results.

As pointed out by Lipari and Lusignoli [43, 44] very often the minijet models does not include in a proper way the possibility of diffractive dissociation. The physical concepts behind this type of process is that hadrons are compounded by punctual particles collectively called partons, which means that in a single hadron-hadron collision there are several multiple parton interactions where each one occurs with different probability and undergoes unequal absorptions. Therefore, the diffractive dissociation is a consequence of the fluctuating structure of hadrons. An approach to explain the existence of inelastic diffraction in terms of the eigenstates of the scattering operator was

*Electronic address: mateus.broilo@ufrgs.br
†Electronic address: barros@ufpel.edu.br
‡Electronic address: pvrgsilva@ufpel.edu.br

proposed many decades ago by Good and Walker [45] and later developed by Miettinen and Pumplin [46] assuming that these eigenstates are associated with the QCD parton states. Following the GW approach many groups were able to include diffraction effects in their formalism by means of multi-channel eikonalized amplitudes [21, 22, 43, 44, 47–53]. Very recently Gonçalves *et al.* [54] following the MP approach have extended the model for diffractive pp collisions to pA interactions at high energies.

With this background in mind, the aim of this paper is to extend the work performed by Lipari and Lusignoli [43, 44] where they have suggested an alternative method, but equivalent to a multi-channel eikonal one as they claim, to introduce diffraction in an eikonal formalism where only the projectile presents a substructure. We explore an eikonalized model based on perturbative QCD in order to describe the total cross-section, $\sigma_{\rm tot}(s)$, and we give predictions to elastic and diffractive cross sections as well as the ρ-parameter, in both pp and antiproton-proton ($\bar{p}p$) channels. We make the assumption that the elastic scattering amplitude is purely imaginary which implies that the opacity and eikonal functions are real. However, we can always relate the real and imaginary parts of the amplitude by means of appropriated dispersion relations. Here we also explore the asymptotic high-energy effects of updated sets of parton distribution functions (PDFs) CTEQ6L [55], CT14 [56] and MMHT [57].

The paper organized as follows...

II. THE MINIJET MODEL

The description of high-energy hadronic interactions must be compatible with the analicity and unitarity properties of the S-matrix. The unitarity condition can be written in the impact parameter representation by the following relation

$$2\,{\rm Re}\,\Gamma(s,b) = |\Gamma(s,b)|^2 + G_{\rm in}(s,b), \tag{1}$$

where $\Gamma(s,b)$ and $G_{\rm in}(s,b)$ are the profile and inelastic overlap functions, respectively. The former describes the resulting effects of absorption from the opening of the inelastic channels and the latter represents the contribution from all inelastic channels. Moreover, the unitarity constraint is satisfied simply by introducing eikonalized amplitudes. In this picture, the profile function is conveniently written as $\Gamma(s,b) = 1 - e^{-\chi(s,b)}$, where $\chi(s,b)$ is the eikonal function. Therefore, in an eikonal representation the elastic scattering amplitude is given by

$$F(s,t) = i\int_0^\infty db\, b\, J_0(b\sqrt{-t})\left[1 - e^{-\chi(s,b)}\right], \tag{2}$$

where s is the CM energy-squared, b is the impact parameter and t is the usual Mandelstam variable.

In this picture, the normalization of elastic amplitudes is such that

$$\frac{d\sigma_{\rm el}}{dt}(s,t) = \pi|F(s,t)|^2, \tag{3}$$

whereas the total cross-section is obtained by means of the optical theorem together with the unitarity condition,

$$\sigma_{\rm tot}(s) = 4\pi\,{\rm Im}\,F(s,t=0) = 4\pi\int_0^\infty db\, b\ {\rm Re}\,\Gamma(s,b), \tag{4}$$

and the elastic and inelastic cross sections are respectively written as

$$\sigma_{\rm el}(s) = 2\pi\int_0^\infty db\, b\,|\Gamma(s,b)|^2, \tag{5}$$

$$\sigma_{\rm in}(s) = \sigma_{\rm tot}(s) - \sigma_{\rm el}(s) = 2\pi\int_0^\infty db\, b\, G_{\rm in}(s,b). \tag{6}$$

As for the case of the ratio ρ of the real-to-imaginary part of the forward elastic scattering amplitude,

$$\sigma_{\rm tot}(s)\rho(s) = 4\pi\,{\rm Re}\,F(s,t=0) = 4\pi\int_0^\infty db\, b\ {\rm Im}\,\Gamma(s,b), \tag{7}$$

the real part of the amplitude can be obtained by means of a singly-subtracted Integral Dispersion Relations (IDR) [58, 59],

$$\frac{\mathrm{Re}\, F_+(s)}{s} = \frac{\mathcal{C}}{s} + \frac{2s}{\pi} P \int_{s_{\rm th}}^{\infty} ds' \left[\frac{1}{s'^2 - s^2}\right] \frac{\mathrm{Im}\, F_+(s')}{s'}, \tag{8}$$

$$\frac{\mathrm{Re}\, F_-(s)}{s} = \frac{2}{\pi} P \int_{s_{\rm th}}^{\infty} ds' \left[\frac{s'}{s'^2 - s^2}\right] \frac{\mathrm{Im}\, F_-(s')}{s'} \ , \tag{9}$$

where $s_{\rm th} = 4m_p^2 = 3.521$ GeV^2 represents the lower energy threshold, $\mathcal{C}$ is the subtraction constant and $F_\pm$ are the crossing even (+) and odd (-) amplitudes related to the physical amplitudes by

$$F_\pm = \frac{1}{2}(F_{pp} \pm F_{\bar{p}p}). \tag{10}$$

Despite the fact that the underlying soft, nonpertubative, physics plays a key part in a consistent description of hadron-hadron processes, the observed increase of hadronic cross sections in minijet models is strictly associated with hard parton-parton scatterings inside the hadrons. This behavior can be introduced by assuming that the eikonal functions for pp and $\bar{p}p$ scatterings are additive with respect soft and hard partonic interactions in the hadron-hadron collision. This is still an open question in QCD-based models, but it also reassembles a possible way to decouple the nonperturbative from the perturbative region. With this background in mind, the eikonal function is given by the following expression

$$\chi(s,b) = \chi_{\rm soft}(s,b) + \chi_{\rm hard}(s,b) = \frac{1}{2}\,\sigma_{\rm eik}(s) W(b), \tag{11}$$

where the eikonal cross-section splits both QCD regions and $W(b)$ is the overlap partonic density which represents the internal hadronic matter distribution.

The *l.h.s.* of Eq. (11) deserves further comments. It states the factorization of the eikonal function, introduced by Durand and Pi [26, 27] and considered in several analysis, *e.g.* [24, 25, 31, 34, 60]. From the point of view of the hadron scattering amplitude, it is expected that the eikonal function depends on how the partons are distributed inside the hadron in the b-plane and on the intensity of the parton-parton interactions. Collisions at different impact parameters will result in different contributions to the amplitude, depending on the number of partons in each of the interacting hadrons. In principle, the partons distribution in b-plane can be modelled by the overlap of hadronic matter in the collision $W(s,b)$, which is related to the Fourier transform of the hadron form factor. On the other hand, the intensity is expected to be determined by the dynamics of the interaction, *i.e.* by the cross-section $\sigma_{\rm eik}(s,b)$ that describes the interaction between the incident hadrons for a given center of mass energy $\sqrt{s}$ and impact parameter b. The factorization *Anzats* assumes that $W(s,b)$ depends only on b, while $\sigma_{\rm eik}(s,b)$ is a function of energy only. Therefore, it is assumed that $\chi(s,b) \propto \sigma_{\rm eik}(s) W(b)$. We note that the factorization or not of the impact parameter and energy dependencies in the description of the eikonal is one important aspect that can be improved in the future, considering *e.g.* the description of the cross-section $\sigma(s,b)$ in terms of the generalized parton distributions, which provide information about how partons are distributed in the plane transverse to the direction in which the hadron is moving (for a review *cf. e.g.* Ref. [61]).

Since $\sigma_{\rm eik}$ must contain information from both the perturbative and nonpertubative regimes of QCD, we will assume that it can be written as a combination of hard and soft contributions

$$\sigma_{\rm eik}(s) = \sigma_{\rm pQCD}(s) + \sigma_{\rm soft}(s), \tag{12}$$

where $\sigma_{\rm pQCD}$ accounts for the mid and high-energy behavior of the elastic scattering amplitude, whilst the $\sigma_{\rm soft}$ is expected to be meaningful only at low energies. Therefore, it is enough to consider that the soft sector can be written by means of a parametrization based on Regge-Gribov pehonomenology. Thus we take

$$\sigma_{\rm soft}(s) = A_1 \left(s/s_0\right)^{-\delta_1} \pm A_2 \left(s/s_0\right)^{-\delta_2} + \sigma_0 \ , \tag{13}$$

where the plus and minus signs correspond to $\bar{p}p$ and pp scatterings, respectively. Furthermore, in the present analysis A_1, A_2, δ_1, δ_2 and σ_0 are fitting parameters and we assume $s_0 = 25$ GeV^2. The first and second terms correspond to even and odd-under-crossing Reggeon exchange, respectively, and σ_0 is associated with the critical Pomeron exchange. Bearing in mind that these Reggeons does not appear directly in the Born-level amplitudes, they must be seen as effective contributions.

The hard sector, which in fact is responsible for the high-energy dynamics, will be expressed by means of the minijet cross-section obtained using perturbative QCD. More specifically, it is obtained through the convolution of the elementary cross-section for the QCD subprocesses respectively with their partonic distributions as follows

$$\begin{aligned}\sigma_{\rm pQCD}(s) &= \sigma_{\rm minijet}(s) \\ &= \sum_{i,j=q,\bar{q},g} \frac{1}{1+\delta_{ij}} \int_0^1 dx_1 \int_0^1 dx_2 \int_{Q^2_{min}}^{\infty} d|\hat{t}| \, \frac{d\hat{\sigma}_{ij}}{d|\hat{t}|}(\hat{s},\hat{t}) \times f_{i/P}(x_1,|\hat{t}|)\, f_{j/T}(x_2,|\hat{t}|)\, \Theta\left(\frac{\hat{s}}{2}-|\hat{t}|\right) , \quad (14)\end{aligned}$$

where x_1 and x_2 are the momentum fractions of the partons inside of hadrons P and T, $\hat{s}$ and $\hat{t}$ are the Mandelstam variables for the partonic collision, $d\hat{\sigma}_{ij}/d|\hat{t}|$ is the differential cross-section for ij scattering, and $f_{i/h}$ stands for the PDFs of the hadron h. The integration over $|\hat{t}|$ satisfy the physical condition $\hat{s} > 2|\hat{t}| > 2Q^2_{min}$, where $\hat{s} = x_1 x_2 s$ and Q^2_{min} is the minimal momentum transfer in the hard scattering, here assumed to be 1.69 GeV^2. Since the gluon distribution becomes dominant in the $x \to 0$ asymptotic regime, we will include in our calculations all process with at least one gluon in the initial state, *i.e.* we select the processes $gg \to gg$ (gluon-gluon fusion), $qg \to qg$ and $\bar{q}g \to \bar{q}g$ (quark-gluon scattering) and for completeness $gg \to \bar{q}q$ (gluon fusion into a quark pair) [33–35]. However, these subprocesses at low transferred momenta are plagued by infrared divergences and must be properly regularized. To tame these divergences we follow the dynamical gluon mass approach proposed by Luna *et al.* [31–35].

In high-energy analyses carried out by models based on the QCD parton model it is necessary to make sense `([Paulo] "sense" parece estranho. Não seria "use"?)` **([Mateus] de fato está mal, mas parece que o "use"também não encaixa aqui.)** of the partonic distribution inside hadrons. Presently, there are many available PDFs sets, but in our investigation we shall focus to investigate the effects of some leading-order updated parametrizations, such as one pre-LHC, namely CTEQ6L [55], and two post-LHC fine-tunned sets, namely CT14 [56] and MMHT [57]. For a recent study *cf.* Ref. [34].

Regarding the overlap density, it is well known that in the QCD parton model the soft and hard sector must not present the same b-dependence, since the former is associated with valence quarks interactions whilst the latter are mainly dominated by gluons. However, the simplest hypothesis is to assume that the partonic spatial distributions in both sectors are described by the same b-perfil. This is a very crude approximation, but it serves as an initial toy model. Therefore, inspired by the proton's charge distribution [26, 27], we assume that both soft and hard overlap densities comes from the charge dipole approximation to the form factors of the colliding hadrons. Thus, $W(b)$, which is the Fourier transform of the hadron form factor, is given by

$$W(b) = \frac{b^3}{96\pi r_0^5} K_3(b/r_0), \quad (15)$$

where for simplicity we use $r_0 = 1.0$ GeV^{-1} and $K_3(x)$ is the modified Bessel function of second kind.

It is most noteworthy that Eq. (1) physically tell us that there is no scattering process that can be uniquely inelastic, since the elastic amplitude indeed receives contributions from both elastic and inelastic channels. This is the shadowing property, *i.e.* within an optical analogy the elastic amplitude is the shadow of the inelastic scattering. Meanwhile, the inelastic overlap function in Eq. (6), $G_{\rm in}(s,b) = 1 - e^{-2\chi(s,b)}$, is interpreted as the probability that at least one hadron is broken up in a collision at impact parameter b. In parton language it means the probability that at least one elementary interaction occurs in the collision process. In addition this idea is basically connected to the fact that different number of interactions takes place in distinct impact parameter b. For this reason, the eikonal function is usually expressed in terms of the average number of interactions $n(s,b)$ in a collision at a given b-value and energy s,

$$2\chi(s,b) = \langle n(s,b) \rangle, \quad (16)$$

where small (large) b corresponds to more (less) interactions. On one hand, notice that by considering this representation in the above expression, the profile function in the eikonal picture is then determined by $\langle n(s,b) \rangle$ and fully describes the elastic scattering. On the other hand it does not take into account different possibilities of elementary interaction configurations and thus the present form of this minijet model can not be used to treat in a reliable way the inelastic diffraction process.

III. GOOD-WALKER APPROACH

Diffractive scattering is usually described within the Good and Walker approach [45], in which the physical state of the incoming hadron $|H\rangle$ is written in terms of the eigenstates of the scattering operator $\hat{T}$, $\{|\psi_k\rangle\}$, with $\mathrm{Im}\,\hat{T}|\psi_k\rangle =$

$t_k|\psi_k\rangle$. Moreover, these eigenstates can only go through elastic scattering and each one present different intensity of interaction. It is this difference that originates the dissociation of the beam particle resulting in diffractive excitation.

Since the eigenstates form a complete set of orthogonal states we can write $|H\rangle = \sum_k C_k|\psi_k\rangle$. So that for the elastic scattering we have

$$\langle H|\hat{T}|H\rangle = \sum_k |C_k|^2 t_k = \langle t\rangle. \tag{17}$$

Therefore, the elastic differential cross-section is given by

$$\frac{d^2\sigma_{\rm el}}{d^2b} = \langle t\rangle^2, \tag{18}$$

where b is the impact parameter of the collision and we have assumed that the eigenstates are purely imaginary.

By means of the optical theorem, the total cross-section distribution in b-space is

$$\frac{d^2\sigma_{\rm tot}}{d^2b} = 2\langle t\rangle. \tag{19}$$

Finally, the dissociative differential cross-section is given by

$$\frac{d^2\sigma_{\rm diff}}{d^2b} = \sum_{P\neq H} |\langle P|\hat{T}|H\rangle|^2, \tag{20}$$

where the summation is over all possible particles P in the final states, excluding the initial hadron H, which would correspond to elastic scattering. It is straight forward to show that

$$\frac{d^2\sigma_{\rm diff}}{d^2b} = \langle t^2\rangle - \langle t\rangle^2, \tag{21}$$

i.e., the dissociation cross sections is given by the variance of the eigenvalues.

The Good-Walker approach gives us a set of tools to calculate the cross sections, but do not include the dynamics of the scattering. For this, we must consider a model for the hadronic scattering in order to be able to calculate the cross sections.

A. The Lipari-Lusignoli model for the scattering eigenstates

In this work, we consider the model proposed by Lipari and Lusignoli [43], briefly reviewed in this section. First, recall that $|C_k|^2$, in equations above, is associated to the probability of finding the eigenstate $|\psi_k\rangle$ in the beam particle state, and consequently, it is associated to the configurations of the internal degrees of freedom of the particle. The authors of Ref.[43] consider that each particle, at the instant of interaction, has a configuration $\mathbb{C}_1$ and $\mathbb{C}_2$, for beam and target respectively, which are elements of a set of configurations $\{\mathbb{C}_1\}$ and $\{\mathbb{C}_2\}$. Each configuration has a probability associated, $P_h(\mathbb{C}_i)$, in the same sense that $|C_k|^2$ is the probability associated to $|\psi_k\rangle$. With this, we can make the following association in all Good-Walker formulae

$$\sum_j |C_j|^2 \to \int d\mathbb{C}_1 \int d\mathbb{C}_2 P_{h1}(\mathbb{C}_1) P_{h2}(\mathbb{C}_2), \tag{22}$$

where it is assumed that all possible configurations can be represented by a continuum distribution.

Considering the partonic structure of the interacting hadrons, we expect that the number of elementary interactions will depend on the impact parameter of the collision and on the configurations $\mathbb{C}_1$ and $\mathbb{C}_2$ of the hadrons, which we shall denote by the function $n(s, b, \mathbb{C}_1, \mathbb{C}_2)$. We also expect that the amplitude eigenstates, at leading order, follows $t(s, b, \mathbb{C}_1, \mathbb{C}_2) \approx n(s, b, \mathbb{C}_1, \mathbb{C}_2)$. In order to take into account the multiple interactions between the partons, we will assume that $t(s, b, \mathbb{C}_1, \mathbb{C}_2)$ is given by the eikonal form

$$t(s, b, \mathbb{C}_1, \mathbb{C}_2) = 1 - \exp\left[-\frac{n(s, b, \mathbb{C}_1, \mathbb{C}_2)}{2}\right], \tag{23}$$

so that the eikonal function, Eq. (11), is $\chi(s, b, \mathbb{C}_1, \mathbb{C}_2) = n(s, b, \mathbb{C}_1, \mathbb{C}_2)/2$.

It is also assumed that the energy and impact parameter dependency of the n function can be factorized from the configurations of the particles, $n(s,b,\mathbb{C}_1,\mathbb{C}_2) = \langle n(s,b)\rangle \alpha(\mathbb{C}_1,\mathbb{C}_2)$, where $\langle n(s,b)\rangle$ is the average number of interactions and the function $\alpha(\mathbb{C}_1,\mathbb{C}_2)$ associates an unique real positive number for each combination of $\mathbb{C}_1$ and $\mathbb{C}_2$. TTherefore, $\alpha(\mathbb{C}_1,\mathbb{C}_2)$ works as works as a mapping from the set of configurations to the set of real positive numbers.

This factorization allows us to write the integrals over the particle configurations in terms of an integral over the real number α by defining the probability distribution $p(\alpha)$:

$$p(\alpha) = \int d\mathbb{C}_1 \int d\mathbb{C}_2 P_{h1}(\mathbb{C}_1) P_{h2}(\mathbb{C}_2) \delta[\alpha(\mathbb{C}_1,\mathbb{C}_2) - \alpha], \tag{24}$$

which describes the fluctuations inside the hadrons and that must satisfy

$$\int_0^\infty d\alpha p(\alpha) = 1; \quad \int_0^\infty d\alpha \alpha p(\alpha) = 1. \tag{25}$$

These constraints follow from the normalization of $P_h(\mathbb{C})$,

$$\int d\mathbb{C} P_h(\mathbb{C}) = 1, \tag{26}$$

and from the definitions of average value of the number of elementary interactions,

$$\int d\mathbb{C}_1 \int d\mathbb{C}_2 P_{h1}(\mathbb{C}_1) P_{h2}(\mathbb{C}_2) n(s,b,\mathbb{C}_1,\mathbb{C}_2) = \langle n(s,b)\rangle. \tag{27}$$

The form of the probability distribution $p(\alpha)$ is still an open problem. However, this distribution must be defined for positive values of its variable (α) and we expect that it has the appropriate limit, $p(\alpha) \to \delta(\alpha - 1)$, when its variance goes to zero, which corresponds to the case of no-fluctuations. It is also interesting to have an analytical structure that allows us, in some extent, to obtain analytical (closed) expressions. The gamma distribution, with variance w,

$$p(\alpha) = \frac{1}{w\Gamma(1/w)} \left(\frac{\alpha}{w}\right)^{-1+1/w} e^{-\alpha/w} , \tag{28}$$

also used in other analysis [43, 62], has the aforementioned properties and it will be our choice in this work. Moreoever, it is straightforward to show that Eq. (28) satisfies the constraints of Eq. (25) and that for $w \to 0$ it shows the expected limit, corresponding to the case of no-fluctuations which implies no dissociative process. In this limit, we also recover the single-channel eikonal model, discussed in Sec. II.

Finally, the average values $\langle t\rangle$ and $\langle t^2\rangle$ are given by

$$\langle t\rangle = 1 - \left(1 + \frac{\langle n(s,b)\rangle w}{2}\right)^{-1/w}, \tag{29}$$

$$\langle t^2\rangle = (1 + \langle n(s,b)\rangle w)^{-1/w} - \left(1 + \frac{\langle n(s,b)\rangle w}{2}\right)^{-2/w}. \tag{30}$$

Finally, we must consider a model to $\langle n(s,b)\rangle$. The treatment of the average number of elementary interactions is an open problem in the literature. However, since in the present model, $\langle n(s,b)\rangle$ is directly related to the eikonal function $\chi(s,b)$, we will assume the *Ansatz* of Eq. (11), *i.e.*, the average number of interactions can be factorized in two parts: the overlap function that depends on b only and describes how the partons are distributed inside the hadron in the b-plane and the eikonal cross-section (a function of energy only) that describes the interaction between the interacting hadrons at a given CM energy $\sqrt{s}$. Following the discussion of Sec. II, we will consider

$$\langle n(s,b)\rangle = \sigma_{\rm eik}(s) \frac{b^3}{96\pi r_0^5} K_3(b/r_0), \tag{31}$$

where the eikonal cross section is given by Eqs. (12)-(14).

PDF	CTEQ6L	CT14	MMHT
w	2.51 ± 0.12	1.83 ± 0.10	3.01 ± 0.13
A_1 [mb]	36.6 ± 3.3	29.8 ± 2.7	42.2 ± 3.8
δ_1	1.45 ± 0.11	1.45 ± 0.11	1.49 ± 0.11
A_2 [mb]	31.7 ± 2.2	26.0 ± 1.8	36.2 ± 2.5
δ_2	0.585 ± 0.045	0.582 ± 0.044	0.583 ± 0.044
σ_0 [mb]	105.7 ± 2.6	91.7 ± 2.2	116.6 ± 3.1
χ^2/ν	3.80	3.75	4.84

TABLE I: Best fit parameters to $\sigma_{\rm tot}$ from pp and $\bar{p}p$ scatterings with PDFs CTEQ6L [55], CT14 [56] and MMHT [57]. The quality fit estimator chi-squared per degree-of-freedom, χ^2/ν, are also included where $\nu = 171$ stands for the number of degrees of freedom.

IV. RESULTS

In order to determine the parameters of the model, w, A_1, A_2, δ_1, δ_2 and σ_0 we consider fits to experimental data for the pp and $\bar{p}p$ total cross sections. The dataset comprise data on $\sigma_{\rm tot}$ obtained only in accelerator experiments covering the energy range from 5 GeV to 13 TeV. Data below 1.8 TeV were obtained from the Particle Data Group [36], while for the LHC energies, we included data obtained by TOTEM Collaboration in the energies of 2.76, 7, 8 and 13 TeV [1, 2, 37–40] and data by ATLAS Collaboration at 7 and 8 TeV [41, 42]. Statistical and systematical uncertainties were added in quadrature.

The model has six free parameters, being five of them associated to the description of the soft cross section. All fits were performed using the class TMinuit from ROOT Framework [**?**] through the MIGRAD algorithm. We consider a χ^2 fitting procedure where the data reduction assumes an interval $\chi^2 - \chi^2_{min} = 7.04$ corresponding, in the case of normal errors, to the projection of the χ^2 hypersurface containing 68.3% of probability, namely uncertainties in the free parameters with 1σ of confidence level.

Notice that $\sigma_{\rm tot}$ is determined by the average of the eigenvalues, Eq. (19), therefore it is less sensitive to parameter w, which determines $p(\alpha)$, compared to the single diffractive cross section, that is given by the variance of the eigenvalues. However, the data of $\sigma_{\rm tot}$ consists of one of the best dataset available, considering the large energy range covered and the precision of the data, especially at high energies. Moreover, as the current precision of the experimental data for $\sigma_{\rm SD}$ is still small, we have chosen not include it in our fit. Nevertheless, it is important to emphasize that we have verified that the description of $\sigma_{\rm tot}$ is sensitive to the description of $p(\alpha)$, by estimating the total cross section assuming different values of the parameter w, while keeping fixed the other parameters that determine the soft cross section.

The parameters determined in fits to $\sigma_{\rm tot}$ data are displayed in Table I. In Figure 1 we show the comparison of experimental data with the fit results for the three PDF sets considered. We see that CT14 and CTEQ6L give similar descriptions to $\sigma_{\rm tot}$ in the entire energy range considered. On the other hand, the MMHT result presents a different increase rate with energy and it crosses the CT14 and CTEQ6L results at approximately 7 TeV. The differences become evident at energies higher than 100 GeV.

Our predictions to $\sigma_{\rm el}$ and $\sigma_{\rm diff}$ are presented, respectively, in left and right panel of Fig. 2. The CT14 set shows the largest magnitude of $\sigma_{\rm el}$ compared with the others and MMHT the lowest. Similar to the total cross section, $\sigma_{\rm el}$ from CT14 and CTEQ6L present similar increase rate but now they differ in the magnitude. The TOTEM data for $\sigma_{\rm el}$ are better described by the result obtained with CTEQ6L. In respect to $\sigma_{\rm diff}$, the prediction with CT14 presents smaller magnitude when compared to the other cases. The larger values are those obtained with MMHT.

The eikonal cross-section, for all cases, is presented in the left panel of Fig. 3 and the soft and hard components in the right panel of the same figure. As expected, the soft contribution dominates at low energies and becomes constant (σ_0) as the energy increases. Moreover, by the energy of $\sqrt{s} \sim 1$ TeV, the hard (pQCD) component is already dominant in the eikonal cross-section.

Using IDR, Eqs.(8) and (9), we are able to calculate the real part of the forward amplitude and, consequently, the ρ-parameter. In order to do so, we need to known the subtraction constant $\mathcal{C}$, which can be obtained in a global fit to $\sigma_{\rm tot}$ and ρ data. However, since this constant only contributes at low energies, we do not expect that it influences our predictions for high energies. Therefore, we set $\mathcal{C} = 0$ to obtain the predictions to ρ parameter showed in the left panel of Fig. 4. All cases predict a value at 13 TeV larger than the measurements.

Also in Fig. 4, we present in the right panel our prediction to the elastic differential cross-section at 13 TeV in comparison to TOTEM data. For low transferred momenta, all cases equally describe the data, but they fail in mid

and large $|t|$. The differential cross-section is more sensible to the internal structure of the hadron and, consequently, to the overlap function. Therefore, our simplest assumption of using the same overlap function to both soft and hard scattering should be improved to describe, in more details, the structures of the interacting particles in the different scattering regimes.

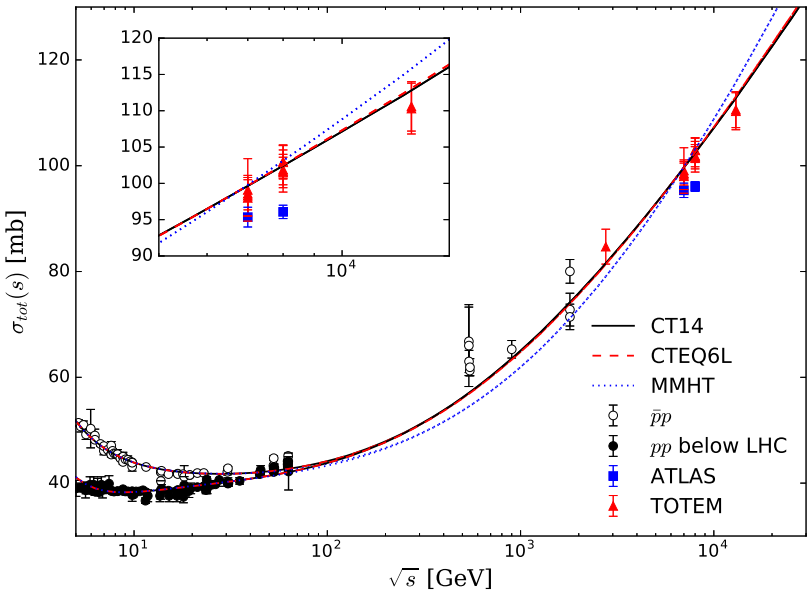

FIG. 1: Fit results to $\sigma_{\rm tot}$ data from pp and $\bar{p}p$ scattering.

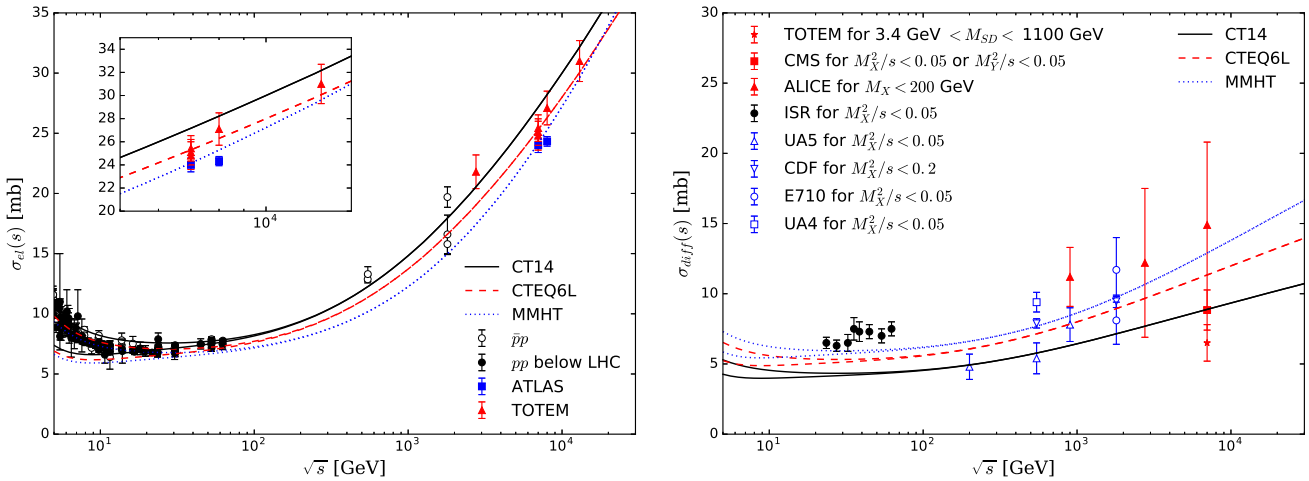

FIG. 2: Predictions for the elastic (left panel) and diffractive dissociation (right panel) cross sections. Data for $\sigma_{\rm el}$ from Refs. [2, 36–39] and $\sigma_{\rm diff}$ from Refs. [63–72].

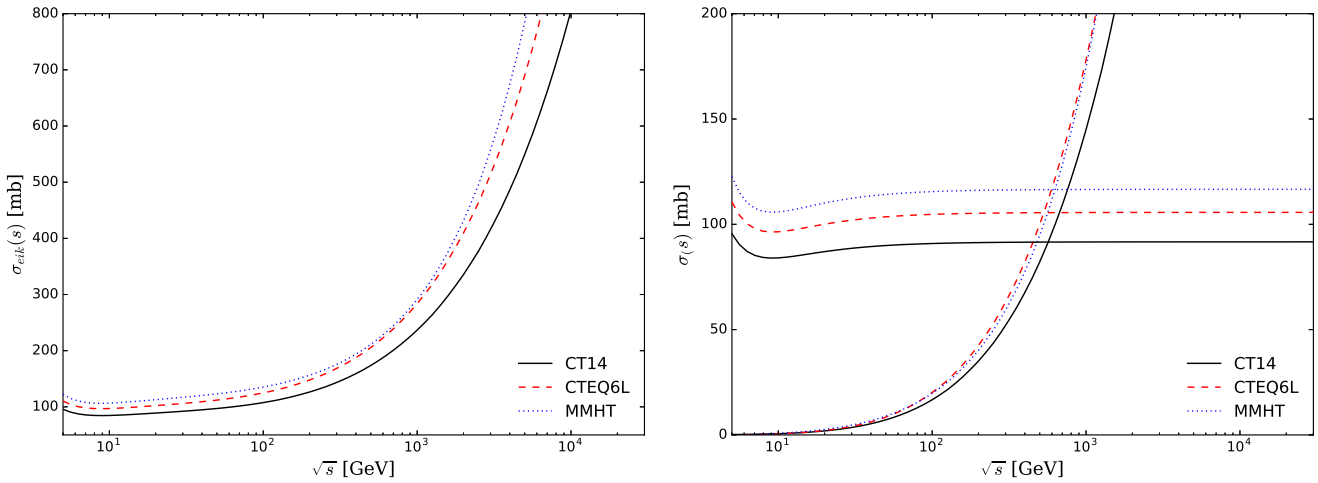

FIG. 3: In the left panel is displayed the $\sigma_{\rm eik}$ and the right one depicts its components. The lower (upper) curves in the right panel relates to the pQCD (soft) components of σ_{eik}. All the curves depicted represents pp only.

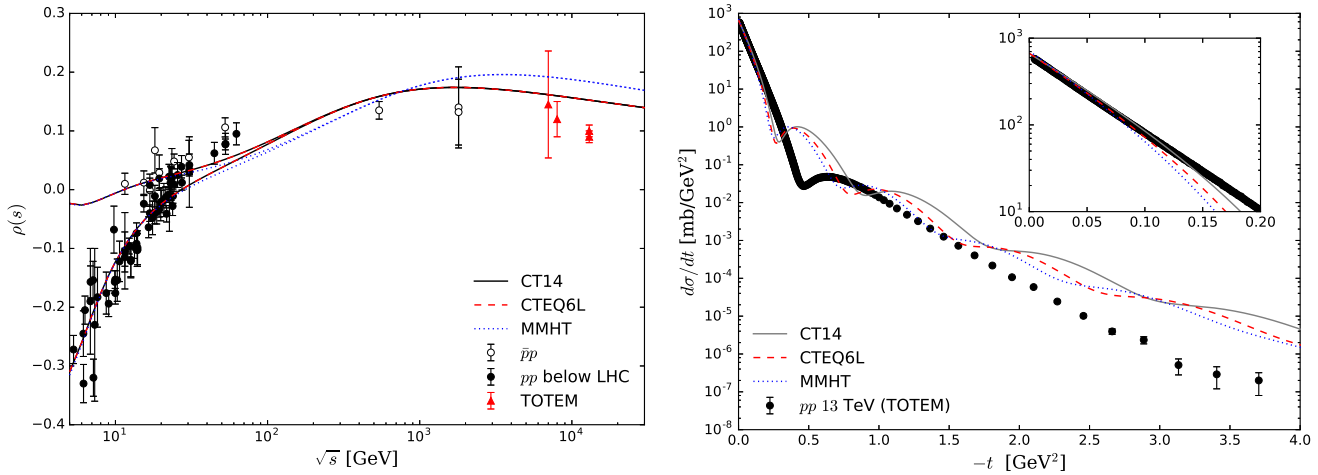

FIG. 4: Predictions for the ρ-parameter data from pp and $\bar{p}p$ scattering (left panel) and elastic differential pp cross-section at 13 TeV (right panel).

V. CONCLUSIONS

The observed increase of hadronic cross sections represents one of the main current trend of interests in both theoretical and experimental Particle Physics. Nonetheless, models based upon QCD represent a possible approach to properly study the high-energy regime of hadronic scaterrings. In this work we have presented a minijet model specially tailored to connect both perturbative and nonperturbative sectors of QCD, where the effects of updated sets of pre and post-LHC fine-tunned PDFs were considered to describe the high-energy partonic interactions. Moreover, we have extended the previous analysis of multiple elementary interactions obtained by Lipari-Lusignoli [43, 44] by considering the fit dataset composed by all the wealth of experimental results for total cross-section in pp and $\bar{p}p$ channels without any sieve procedure. Bearing in mind that the bulk of $\sigma_{\rm tot}$ data presently consists one of the best and most complete datasets covering the high-energy range of pp and $\bar{p}p$ scatterings, we carried out fits to $\sigma_{\rm tot}^{pp,\bar{p}p}$ paying attention to the different forward behaviors implied by distinct partonic distribution inside hadrons, namely CTEQ6L, CT14 and MMHT. The best-fitted parameter to $\sigma_{\rm tot}$ were also used to predict the total elastic and diffractive cross sections. In addition, we have also predicted the ρ-parameter and the differential elastic cross-section. However, it is worth noting that although we were able to accurate describe the current high-energy increase behavior

of the hadronic cross sections experimental data, the poor description of the elastic differential cross section at large transferred momenta indicates that the spatial distribution of the partonic content inside hadrons still must to be improved. Studies on this topic are in progress.

([Paulo] Beleza. Nos próximos dias pretendo ler mais algumas vezes e vou adicionando outras modificações, se necessário.)

([Mateus] Perfeito Paulo! Já implementei muitas das tuas modificações e concordo com todas elas, exceto uma que ainda estou em dúvida. Vou esperar as indicações e mudanças do Victor.)

Acknowledgments

This research was partially supported by the Conselho Nacional de Desenvolvimento Científico e Tecnológico (CNPq), Fundação de Amparo à Pesquisa do Estado do Rio Grande do Sul (FAPERGS) and Instituto Nacional de Ciência e Tecnologia – Física Nuclear e Aplicações (INCT-FNA) (process number 464898/2014-5 and 155628/2018-6).

Extra

[Paulo] Aqui estão as figuras de $d\sigma_{\rm diff}/d^2b$. Como colocar várias energias para diferenes pdfs ficava muito poluido, eu separei em dois casos: evolução em energia para uma PDF e diferentes PDFs para uma energia. Também fiz uma figura mostrando a diferença entre da posição do máximo da distribuição para cada PDF e como evolui com a energia. Acredito que essa diferença é a responsável pela diferente taxa de crescimento apresentada pela MMHT.

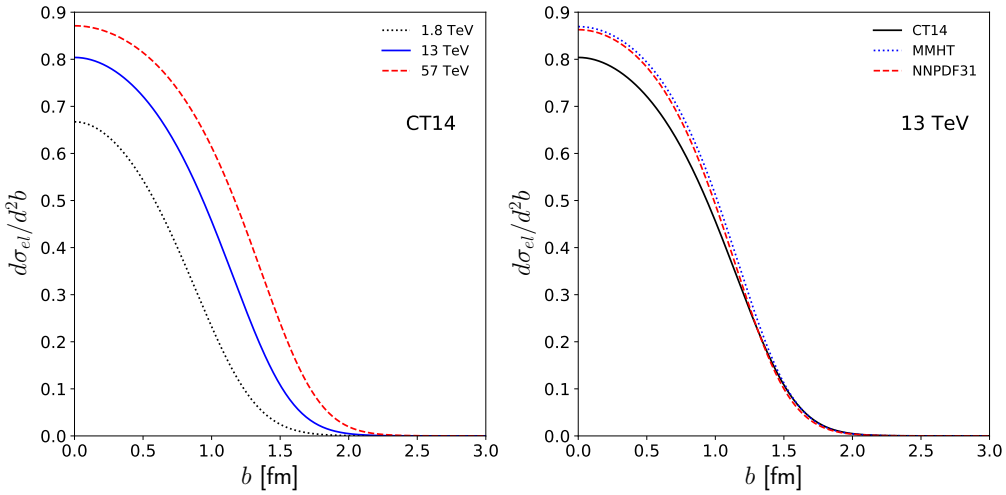

FIG. 5: Energy evolution of $d\sigma_{\rm el}/d^2b$ (left) for CT14 and differences at 13 TeV for three PDFs (right).

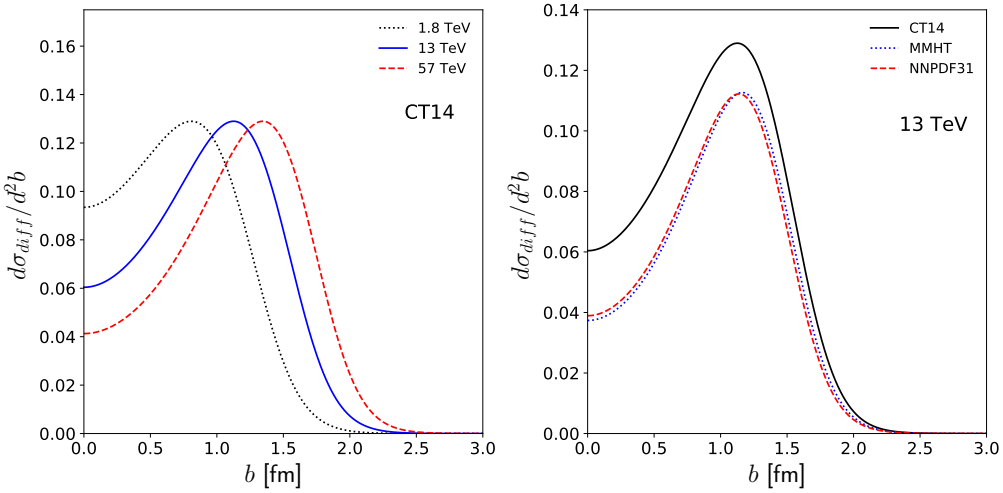

FIG. 6: Energy evolution of $d\sigma_{\rm diff}/d^2b$ (left) for CT14 and differences at 13 TeV for three PDFs (right).

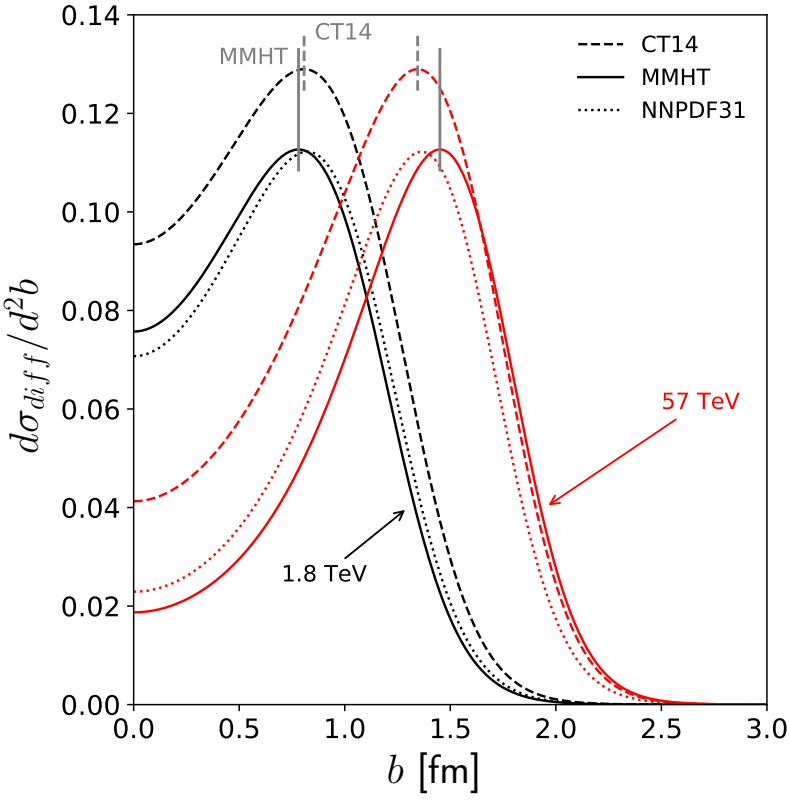

FIG. 7: Energy evolution of the maximum of $d\sigma_{\rm diff}/d^2b$ for three PDFs. The vertical lines correspond to the value of b where the distribution is maximum. The maximum for CTEQ6L, not shown, is between MMHT and CT14 at 1.8 TeV and close to the value of CT14 at 57 TeV.

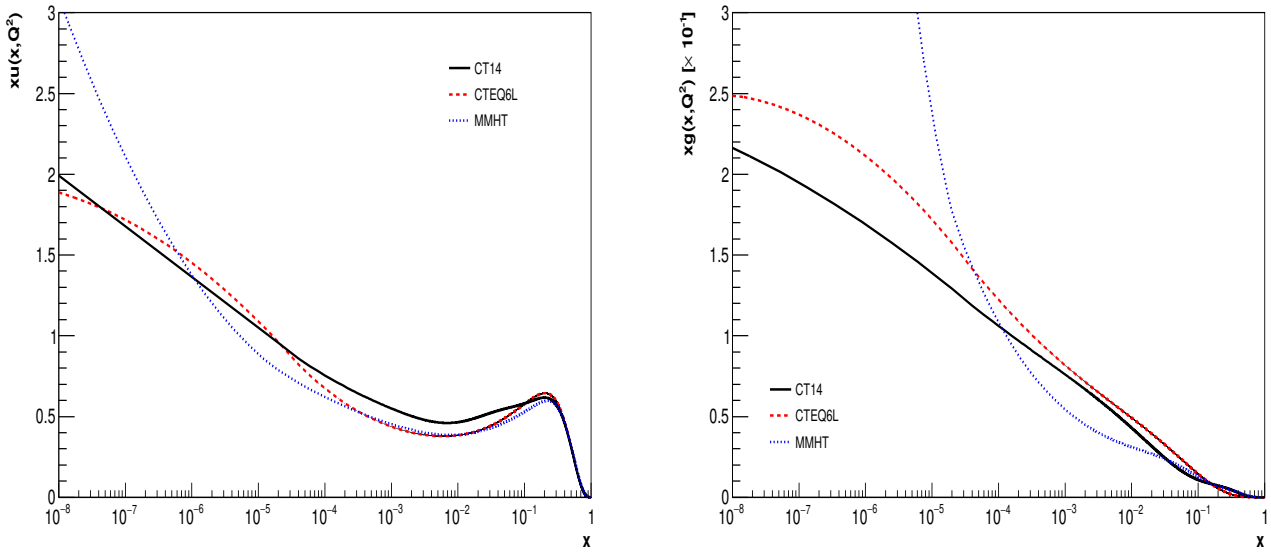

FIG. 8: Up quark and gluon distribution function, $xf(x, Q^2)$, by means of DGLAP evolution for CT14, CTEQ6L and MMHT PDF's considering $Q = Q_{min} = 1.3$ GeV.

[1] G. Antchev et al. (TOTEM), Eur. Phys. J. **C79**, 785 (2019), 1812.04732.
[2] G. Antchev et al. (TOTEM), Eur. Phys. J. **C79**, 103 (2019), 1712.06153.
[3] G. Antchev et al. (TOTEM), Eur. Phys. J. **C79**, 861 (2019), 1812.08283.
[4] G. Antchev et al. (TOTEM), Eur. Phys. J. **C80**, 91 (2020), 1812.08610.
[5] H. Cheng and T. T. Wu, Phys. Rev. Lett. **24**, 1456 (1970).
[6] C. Bourrely, J. Soffer, and T. T. Wu, Phys. Rev. Lett. **54**, 757 (1985).
[7] G. Matthiae, Rept. Prog. Phys. **57**, 743 (1994).
[8] A. Donnachie and P. V. Landshoff, Z. Phys. **C2**, 55 (1979), [Erratum: Z. Phys.C2,372(1979)].
[9] A. Donnachie and P. V. Landshoff, Phys. Lett. **B296**, 227 (1992), hep-ph/9209205.
[10] A. Donnachie and P. V. Landshoff, Phys. Lett. **B727**, 500 (2013), [Erratum: Phys. Lett.B750,669(2015)], 1309.1292.
[11] J. R. Cudell, V. Ezhela, P. Gauron, K. Kang, Yu. V. Kuyanov, S. Lugovsky, B. Nicolescu, and N. Tkachenko, Phys. Rev. **D65**, 074024 (2002), hep-ph/0107219.
[12] M. M. Block and F. Halzen, Phys. Rev. **D86**, 014006 (2012), 1205.5514.
[13] M. M. Block and F. Halzen, Phys. Rev. **D86**, 051504 (2012), 1208.4086.
[14] R. F. Avila, E. G. S. Luna, and M. J. Menon, Phys. Rev. **D67**, 054020 (2003), hep-ph/0212234.
[15] E. G. S. Luna and M. J. Menon, Phys. Lett. **B565**, 123 (2003), hep-ph/0305280.
[16] D. A. Fagundes, M. J. Menon, and P. V. R. G. Silva, Nucl. Phys. **A966**, 185 (2017), 1703.07486.
[17] D. A. Fagundes, M. J. Menon, and P. V. R. G. Silva, Int. J. Mod. Phys. **A32**, 1750184 (2017), 1705.01504.
[18] M. Broilo, E. G. S. Luna, and M. J. Menon, Phys. Lett. **B781**, 616 (2018), 1803.07167.
[19] M. Broilo, E. G. S. Luna, and M. J. Menon, Phys. Rev. **D98**, 074006 (2018), 1807.10337.
[20] R. Fiore, L. L. Jenkovszky, R. Orava, E. Predazzi, A. Prokudin, and O. Selyugin, Int. J. Mod. Phys. **A24**, 2551 (2009), 0810.2902.
[21] E. G. S. Luna, V. A. Khoze, A. D. Martin, and M. G. Ryskin, Eur. Phys. J. **C59**, 1 (2009), 0807.4115.
[22] E. Gotsman, E. M. Levin, and U. Maor, Phys. Rev. **D49**, R4321 (1994), hep-ph/9310257.
[23] P. L'Heureux, B. Margolis, and P. Valin, Phys. Rev. **D32**, 1681 (1985).
[24] B. Margolis, P. Valin, M. M. Block, F. Halzen, and R. S. Fletcher, Phys. Lett. **B213**, 221 (1988).
[25] M. M. Block, E. M. Gregores, F. Halzen, and G. Pancheri, Phys. Rev. **D60**, 054024 (1999), hep-ph/9809403.
[26] L. Durand and H. Pi, Phys. Rev. **D38**, 78 (1988).
[27] L. Durand and H. Pi, Phys. Rev. **D40**, 1436 (1989).
[28] A. Corsetti, A. Grau, G. Pancheri, and Y. N. Srivastava, Phys. Lett. **B382**, 282 (1996), hep-ph/9605314.
[29] D. A. Fagundes, A. Grau, S. Pacetti, G. Pancheri, and Y. N. Srivastava, Phys. Rev. **D88**, 094019 (2013), 1306.0452.
[30] D. A. Fagundes, A. Grau, G. Pancheri, Y. N. Srivastava, and O. Shekhovtsova, Phys. Rev. **D91**, 114011 (2015), 1504.04890.
[31] E. G. S. Luna, A. F. Martini, M. J. Menon, A. Mihara, and A. A. Natale, Phys. Rev. **D72**, 034019 (2005), hep-ph/0507057.

[32] E. G. S. Luna, A. L. dos Santos, and A. A. Natale, Phys. Lett. **B698**, 52 (2011), 1012.4443.
[33] C. A. S. Bahia, M. Broilo, and E. G. S. Luna, Phys. Rev. **D92**, 074039 (2015), 1510.00727.
[34] M. Broilo, D. A. Fagundes, E. G. S. Luna, and M. J. Menon, Eur. Phys. J. **C79**, 1033 (2019), 1906.05932.
[35] M. Broilo, D. A. Fagundes, E. G. S. Luna, and M. J. Menon, Phys. Lett. **B799**, 135047 (2019), 1904.10061.
[36] M. Tanabashi et al. (Particle Data Group), Phys. Rev. **D98**, 030001 (2018).
[37] G. Antchev et al. (TOTEM), EPL **101**, 21004 (2013).
[38] G. Antchev et al. (TOTEM), Phys. Rev. Lett. **111**, 012001 (2013).
[39] G. Antchev et al. (TOTEM), Nucl. Phys. **B899**, 527 (2015), 1503.08111.
[40] G. Antchev et al. (TOTEM), Eur. Phys. J. **C76**, 661 (2016), 1610.00603.
[41] G. Aad et al. (ATLAS), Nucl. Phys. **B889**, 486 (2014), 1408.5778.
[42] M. Aaboud et al. (ATLAS), Phys. Lett. **B761**, 158 (2016), 1607.06605.
[43] P. Lipari and M. Lusignoli, Phys. Rev. **D80**, 074014 (2009), 0908.0495.
[44] P. Lipari and M. Lusignoli, Eur. Phys. J. **C73**, 2630 (2013), 1305.7216.
[45] M. L. Good and W. D. Walker, Phys. Rev. **120**, 1857 (1960).
[46] H. I. Miettinen and J. Pumplin, Phys. Rev. **D18**, 1696 (1978).
[47] A. B. Kaidalov, Phys. Rept. **50**, 157 (1979).
[48] R. S. Fletcher, Phys. Rev. **D46**, 187 (1992).
[49] S. Roesler, R. Engel, and J. Ranft, Z. Phys. **C59**, 481 (1993).
[50] M. G. Ryskin, A. D. Martin, and V. A. Khoze, Eur. Phys. J. **C54**, 199 (2008), 0710.2494.
[51] E. Gotsman, E. Levin, U. Maor, and J. S. Miller, Eur. Phys. J. **C57**, 689 (2008), 0805.2799.
[52] E. Avsar, G. Gustafson, and L. Lonnblad, JHEP **12**, 012 (2007), 0709.1368.
[53] C. Bierlich, G. Gustafson, and L. Lönnblad, JHEP **10**, 139 (2016), 1607.04434.
[54] V. P. Gonçalves, R. P. da Silva, and P. V. R. G. Silva, Phys. Rev. **D100**, 014019 (2019), 1905.00806.
[55] J. Pumplin, D. R. Stump, J. Huston, H. L. Lai, P. M. Nadolsky, and W. K. Tung, JHEP **07**, 012 (2002), hep-ph/0201195.
[56] S. Dulat, T.-J. Hou, J. Gao, M. Guzzi, J. Huston, P. Nadolsky, J. Pumplin, C. Schmidt, D. Stump, and C. P. Yuan, Phys. Rev. **D93**, 033006 (2016), 1506.07443.
[57] L. A. Harland-Lang, A. D. Martin, P. Motylinski, and R. S. Thorne, Eur. Phys. J. **C75**, 204 (2015), 1412.3989.
[58] P. Söding, Physics Letters **8**, 285 (1964), ISSN 0031-9163, URL `http://www.sciencedirect.com/science/article/pii/S0031916364918979`.
[59] M. M. Block and R. N. Cahn, Rev. Mod. Phys. **57**, 563 (1985).
[60] D. A. Fagundes, A. Grau, G. Pancheri, O. Shekhovtsova, and Y. N. Srivastava, Phys. Rev. D **96**, 054010 (2017), 1706.00093.
[61] M. Diehl, Ph.D. thesis (2003), hep-ph/0307382.
[62] H. I. Miettinen and G. H. Thomas, Nucl. Phys. **B166**, 365 (1980).
[63] J. C. M. Armitage et al., Nucl. Phys. **B194**, 365 (1982).
[64] N. Cartiglia (2013), 1305.6131, URL `http://arxiv.org/abs/1305.6131`.
[65] B. Abelev et al. (ALICE), Eur. Phys. J. **C73**, 2456 (2013), 1208.4968.
[66] V. Khachatryan et al. (CMS), Phys. Rev. **D92**, 012003 (2015), 1503.08689.
[67] R. E. Ansorge et al. (UA5), Z. Phys. **C33**, 175 (1986).
[68] G. J. Alner et al. (UA5), Phys. Rept. **154**, 247 (1987).
[69] D. Bernard et al. (UA4), Phys. Lett. **B186**, 227 (1987).
[70] N. A. Amos et al. (E-710), Phys. Lett. **B243**, 158 (1990).
[71] N. A. Amos et al. (E710), Phys. Lett. **B301**, 313 (1993).
[72] F. Abe et al. (CDF), Phys. Rev. **D50**, 5535 (1994).
[73] `https://root.cern.ch/doc/master/classTMinuit.html`